Hindawi
International Journal of Optics
Volume 2021, Article ID 6937072, 8 pages
https://doi.org/10.1155/2021/6937072

Research Article

High-Accuracy Surface Profile Measurement Based on the Vortex Phase-Shifting Interferometry

Donge Zhao,[1,2] **Chaozheng Jia**,[1] **Yayun Ma**,[1] **Xuefeng Yang**,[1] **Bin Zhang**,[1] **and Wenbo Chu**[1]

[1]*School of Information and Communication Engineering, North University of China, Taiyuan 030051, China*
[2]*Shanxi Provincial Research Center for Opto-Electronic Information & Instrument Engineering Technology, North University of China, Taiyuan 030051, China*

Correspondence should be addressed to Donge Zhao; zhaodonge@nuc.edu.cn

Received 29 May 2021; Revised 29 July 2021; Accepted 21 August 2021; Published 3 September 2021

Academic Editor: Stefan Wabnitz

According to the principle of phase-shifting interferometry and spiral phase characteristics of the vortex beam, this article proposes a method for detecting the surface profile of a transparent object, in which the +1 order vortex beam is generated by a spatial light modulator and is taken as the reference light. The influence of the nonlinear phase modulation characteristics of the spatial light modulator on the measurement precision is studied. The results show that nonlinear phase modulation has a great impact on the measurement. Then, the vortex lights with initial phases of 0, $\pi/2$, π, and $3\pi/2$ are used to measure the H-type thin film sample based on the Twyman-Green interference system after correcting the nonlinear phase modulation characteristics. The experimental results show that the measurement error of the surface profile to an object with the theoretical value of 20 nm is 1.146 nm, and the feasibility of the optical vortex phase-shifting technique used to measure the surface profile of an object is verified.

1. Introduction

The new structured light carrying orbital angular momentum (OAM), also known as vortex beam due to its spiral phase structure and phase singularity, is one of the research focuses in optical domain [1–3]. The optical orbital angular momentum theoretically provides an infinite multidimensional orthogonal basis, which can be used for information coding [4] and optical communication [5–7]. Based on its special interference and diffraction characteristics, the research on the OAM detection of the optical communication receiving end is ongoing [8–10]. Vortex light is also effectively used in other fields, such as optical capture [11], superresolution microscopic imaging [12] and measurement [13, 14].

Taking into account the beam quality, conversion efficiency, production cost, and flexibility has always been the goal pursued by the generation of vortex light fields. There are many optical elements used to generate optical vortices, such as spiral phase plates (SPPs) [15, 16], DOEs [17], and optical fibers, among which the preparation and characterization of SPPs have been extensively studied [18, 19]. In the survey field, vortex beams can be generated by the spatial light modulator (SLM) which can perform precise phase-shift operations [20–22]. Combining vortex light phase shift technology and phase unwrapping technology, noncontact, high-resolution, and wide-range measurement applications can be realized, such as micro-deformation, microdisplacement, and refractive index of materials [23]. Sun et al. proposed a new method for in-plane displacement measurement of objects by applying optical vortex phase-shifting into speckle measurement with the speckle interference principle [24]. In addition, Zhang et al. introduced elliptical vortex lens into phase-shifting image-plane digital holography and measured a test target and the multiplaner focal spots of Taiji lens [25]. Meanwhile, Wang et al. measured the three-dimensional refractive index of special optical fibers based on optical vortex-shifting digital holographic microscopy [26]. On the other hand, in the field of surface measurement, Masajada et al. used an optical vortex interferometer to detect the quality of samples by scanning the surface of samples with a focused vortex beam and reported a new method of inspecting

deep microstructures manufactured in transparent media [27]. Serrano-Trujillo et al. presented a common-path interferometer based on the phase singularity of optical vortex beam, which can detect an average surface depth of 179 nm [28].

In this study, a Twyman-Green interferometer is built on the basis of the vortex phase-shifting interferometry principle, and the surface profile distribution of the film sample is measured. By analyzing the nonlinear modulation of SLM which generates vortex beams, the vortex beam with nonlinear phase distribution is simulated, and the results show that the error of measurement results is proportional to the degree of nonlinear phase modulation. Before and after placing the sample in the beam path, four pairs of interferograms between vortex beams and plane waves are recorded by the CCD camera, respectively. Then, phase unwrapping is performed on the acquired images to obtain the three-dimensional structure distribution of the sample. From the measurement results, it can be proved that the vortex beam phase shift technology is feasible in the field of nanometer-scale surface profile measurement.

2. Theoretical Analysis

As a real-time optical information processing device, the spatial light modulator can generate vortex beams quickly and accurately. Here, the expression of ideal vortex beams generated by the liquid crystal spatial light modulator is given by the following formula [29]:

$$E_R = A_R \exp(il\theta)\exp(i\varphi_1), \tag{1}$$

where A_R is the amplitude of vortex beams, l is the topological charge, θ is the azimuth angle of the vortex beam along the vortex axis, and φ_1 is the initial phase.

The complex amplitude expression of the plane wave is

$$E_O = A_O \exp(i\varphi_2), \tag{2}$$

where A_O and φ_2 are the amplitude and the initial phase of the plane wave, respectively.

By changing holograms of SLM, the phase distribution is changed, so phase-shifting can be realized in the measurement process. Using the four-step phase-shifting technique, the shift step δ is $\pi/2$, and the phase is 0, $\pi/2$, π, and $3\pi/2$, respectively. The optical field expression of the intensity in the interference pattern between plane beam and vortex beam is

$$I_{1m} = A_O^2 + A_R^2 + 2A_O A_R \cdot \cos[l\theta + (m-1)\delta + \varphi_1 - \varphi_2]; \quad m = 1, 2, 3, 4. \tag{3}$$

After adding the phase difference $\Delta\varphi$, the expression of interference intensity is

$$I_{2m} = A_O^2 + A_R^2 + 2A_O A_R \cdot \cos[l\theta + (m-1)\delta + \varphi_1 - \varphi_2 + \Delta\varphi]; \quad m = 1, 2, 3, 4. \tag{4}$$

According to Hu's analysis [30], the phase distribution of the object to be measured is

$$\Delta\varphi = arc\tan\frac{(I_{11} - I_{13})(I_{24} - I_{22}) - (I_{14} - I_{12})(I_{21} - I_{23})}{(I_{11} - I_{13})(I_{21} - I_{23}) - (I_{14} - I_{12})(I_{24} - I_{22})}. \tag{5}$$

The relationship between the phase and the actual thickness of object to be measured is

$$\Delta\varphi = \frac{2\pi}{\lambda}(n-1) \times \Delta L, \tag{6}$$

where n is the refractive index, and ΔL is the thickness of the optically transparent sample. Therefore, the profile of the transparent sample can be obtained by converting the two-dimensional distributed phase information into thickness information.

3. Nonlinear Modulation Simulation

The principle of generating vortex beams by SLM is similar to computer holography. On the basis of computer holography, the phase diagram of vortex beam is put into SLM, and the experimental parameters are controlled by the computer in real time, so that vortex beams with different topological charges and initial phase are generated. According to formula (6), it can be seen that the phase difference $\Delta\varphi$ determines the true profile of the sample. The phase accuracy of vortex light is determined by the modulation ability of the SLM, so the nonlinearity of phase modulation will affect the experimental results. Gamma transformation is a common nonlinear modulation. In order to study the influence of nonlinear phase modulation of spatial light modulator on the results, the simulation analysis is conducted through MATLAB in this study. The phase hologram of vortex beam is transformed into the nonlinear gray scale to simulate the nonlinearity of phase modulation. The formula of gamma transformation is

$$S(x, y) = C \cdot g(x, y)^{\gamma}, \tag{7}$$

where C is the proportional constant, and C is set to 255 for 8-bit gray-level bitmap addressing over the 2π range. $g(x, y)$ is the gray-scale distribution function after normalization of the phase diagram of vortex beam (scale the gray-scale range linearly to 0-1). γ is the transformation coefficient, and $S(x, y)$ refers to the gray function after transformation, which is the phase distribution of vortex beam after nonlinear modulation. In linear modulation, the phase of +1 order vortex light generated by SLM shows a linear change from 0 to 2π around the vortex axis, and the gray level of the phase diagram shows linear increase from 0 to 255. Hologram with the nonlinear phase of vortex beam is different, as shown in Figure 1; when $\gamma < 1$, the phase hologram is brighter; otherwise, it is darker. The results show that the transformed phase of vortex beam is exponentially distributed along the axial direction, rather than linearly changing. Figure 2 shows the characteristic curve of nonlinear phase modulation of SLM according to formula (7).

After the transformed phase of vortex beams with different gamma coefficients is obtained, the interference intensity is calculated according to formulas (3) and (4). And

(a) (b) (c)

Figure 1: Phase gray-scale images of +1 vortex beam with different gamma coefficients. (a) $\gamma = 0.6$, (b) $\gamma = 1$, and (c) $\gamma = 1.5$.

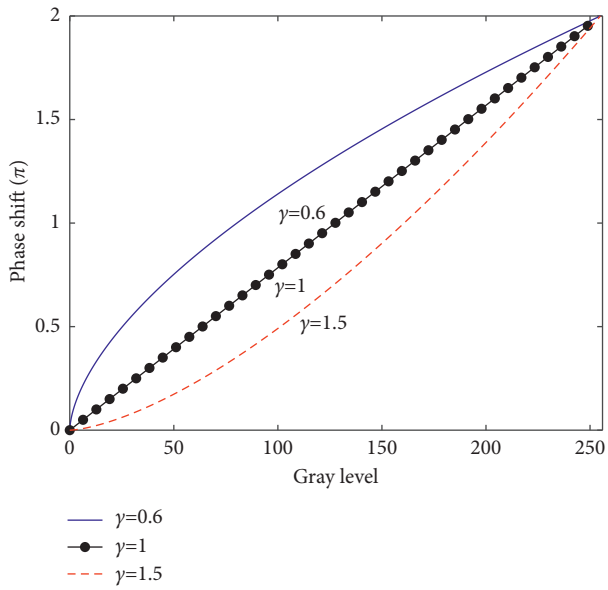

Figure 2: Phase modulation characteristics.

then, the simulated phase distribution can be solved by substituting the interference intensity value in formula (5). In the simulation, the wavelength of the laser is 640 nm, refractive index of sample to be measured is 1.5, and its geometrical thickness ΔL is 20 nm, so its phase value $\Delta\varphi$ is $20\pi/640$, which is approximately equal to 0.1 rad according to formula (6). Finally, the influence of different gamma coefficients on phase error can be analyzed.

According to the results in Figure 3 and Table 1, it can be seen that nonlinear modulation of spatial light modulator has an impact on the measurement. When gamma deviates from 1, the error increases gradually. Therefore, it is necessary to test and eliminate the nonlinear modulation of spatial light modulator before the vortex beam phase-shifting interferometry.

4. Experimental Preoperation and Setup

The simulation in the previous section shows that in order to reduce the measurement error, it is necessary to ensure the accuracy of the phase modulation of SLM. There are many calibration methods for the phase modulation characteristics of LCOS-SLM, among which interferometry is commonly used internationally [31, 32]. After measuring the modulation curve of the input gray-scale and phase response of the SLM, the inverse interpolation method is used to regenerate the look-up table (LUT) corresponding to the driving gray-scale and the input gray-scale. The LUT maps each gray value in the image to a new gray value, so that the SLM correction is completed [33]. In this study, the modulation curve of the LC-SLM are measured by the Twyman-Green interference system. Based on the correlation algorithm [34], the value of interference fringe movement corresponding to a different input gray-scale is calculated, and finally, the relation curve that phase shift varies with the gray level is shown in Figure 4.

The experimental setup for measuring the surface profile of samples based on optical vortex phase-shifting technique is shown in Figure 5. A semiconductor laser is used as a light source, with a wavelength of 640 nm and the power of 2 mW. After the beam expansion system, the diameter of the exiting spot is 10 mm. The intensity is adjusted by the polarizer P1; then, laser beam passes the analyzer P2 (the direction of polarization is aligned with liquid crystal direction of SLM) into beam splitter (BS), and the light is divided into two beams. One beam illuminates the SLM to generate vortex beam as a reference beam. The other beam passes through the object and illuminates the standard mirror (M) as an object beam. The object and reference beam after reflections are recombined by the beam splitter, and the interference fringes are recorded by a CCD camera with a collimator. The spatial light modulator in the experiment is liquid crystal spatial light modulation (PLUTO-NIR-011, HOLOEYE, Germany) with image resolution of 1920×1080, pixel unit size of 8.0 μm, and a response time of 16 ms–200 ms. It is used to generate vortex beams as the reference beam and realize phase-shifting operation by changing the spiral phase distribution of the vortex wavefront. The camera is a monochrome CCD, with active image resolution of 1040×1392 and pixel size of 6.45 μm.

4.1. Experimental Results and Discussion. In the experiment, a 20 nm thick H-shaped silicon dioxide film ($n = 1.515$) [35] plating in a glass sample is measured, and the structure diagram of the sample is shown in Figure 6. In the optical

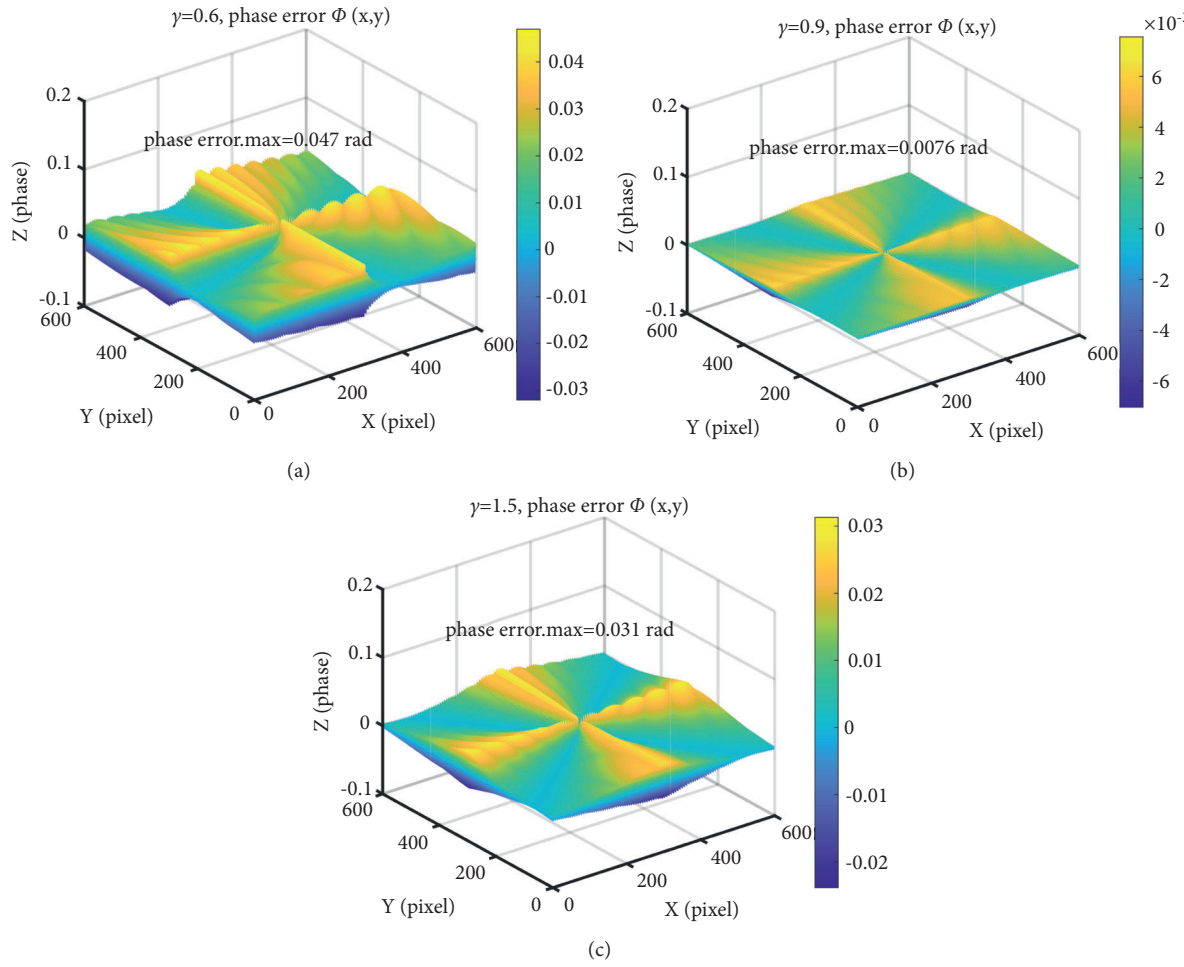

Figure 3: Phase error caused by nonlinear modulation. (a) $\gamma = 0.6$, (b) $\gamma = 0.9$, and (c) $\gamma = 1.5$.

Table 1: Error comparison of the nonlinear modulation with different gamma values.

γ	0.6	0.8	0.9	1.1	1.3	1.5	1.8	2
ΔPhase_max (rad)	0.047	0.017	0.0076	0.0065	0.0188	0.031	0.053	0.071
ΔLength_max (nm)	9.57	3.46	1.55	1.32	3.83	6.32	10.80	14.46
Error rate_max (%)	47	17	7.6	6.5	18.8	31	53	71

path, because the light beam passes through the sample twice, the theoretical phase value of the silicon dioxide film is 0.202 rad, which is calculated by formula (6).

Figureds 77(a)–7(d) show the four interferograms without placing the sample into the experimental system. After placing the sample, four interferograms containing sample information are recorded, as shown in Figures 7(e)–7(h), respectively. Looking at all the images in Figure 7, the distribution of the interference fringes of the vortex beam and the plane beam is characterized by a forked stripe at the center of the interference field, and when the spiral phase of vortex light changes, the interference fringes move relative to the center of the fork.

After substituting the intensity values of eight interferograms into formula (5) for calculation, a phase diagram containing sample information can be obtained, as shown in Figure 8(a). It can be seen from Figure 8(a) that there are obvious steps in the phase diagram. The phase diagram with phase change of such steps is called the wrapped phase. After analysis, the phase step produced in the experiment is caused by the tilt of the sample when it is placed in the optical path. Therefore, it is necessary to unwrap the wrapped phase to obtain the true phase distribution.

After unwrapping operation, the phase distribution diagram obtained is shown in Figure 8(b). The flowchart of image processing in the experiment is shown in Figure 9, which includes image segmentation, binarization, and image filtering. The phase shift algorithm and unwrapping algorithm are used to calculate the phase distribution of the object [36], and then, the phase image is filtered. Finally, the surface profile of the object is obtained.

The three-dimensional structure of the object is shown in Figure 10(a). The calculation of the image in 170th line shows that the phase value of the thin film is 0.186 rad, and

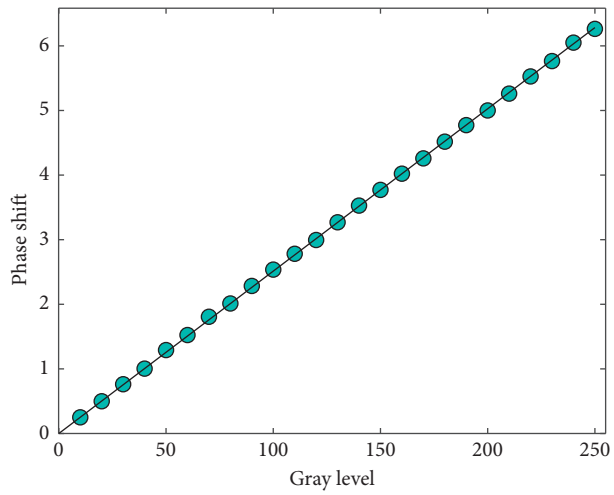

Figure 4: Linear phase modulation characteristics.

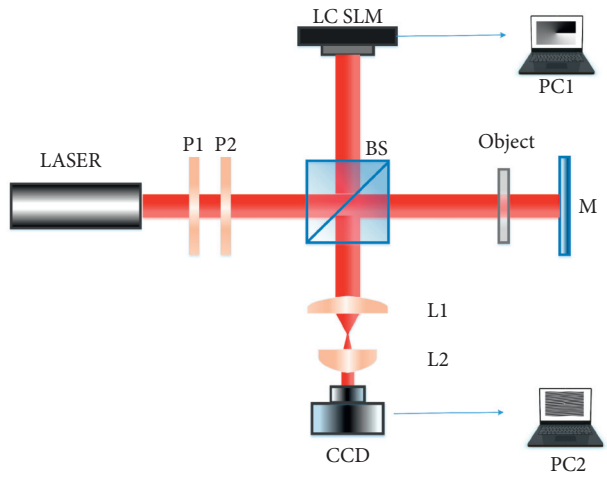

Figure 5: Experimental setup for measuring the surface profile based on optical vortex phase shift. P1, polarizer; P2, analyzer; BS, beam splitter; LC-SLM, liquid crystal spatial light modulator; M, mirror; L1 and L2, collimator; CCD, charge coupled device camera; PC1 and PC2, computers.

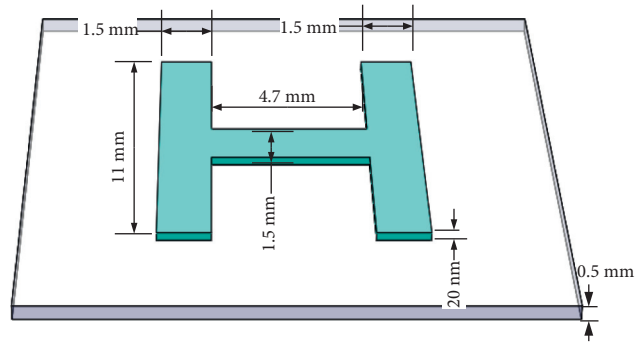

Figure 6: Schematic diagram of the sample structure.

the calculated sample thickness is 18.394 nm, with an error of 1.606 nm from the theoretical value of 20 nm. By averaging the whole H-shaped phase, the thickness and error of the sample calculated by formula (6) are 18.854 nm and 1.146 nm, respectively. The phase value of the 170th line is shown in Figure 10(b). According to the number of pixels

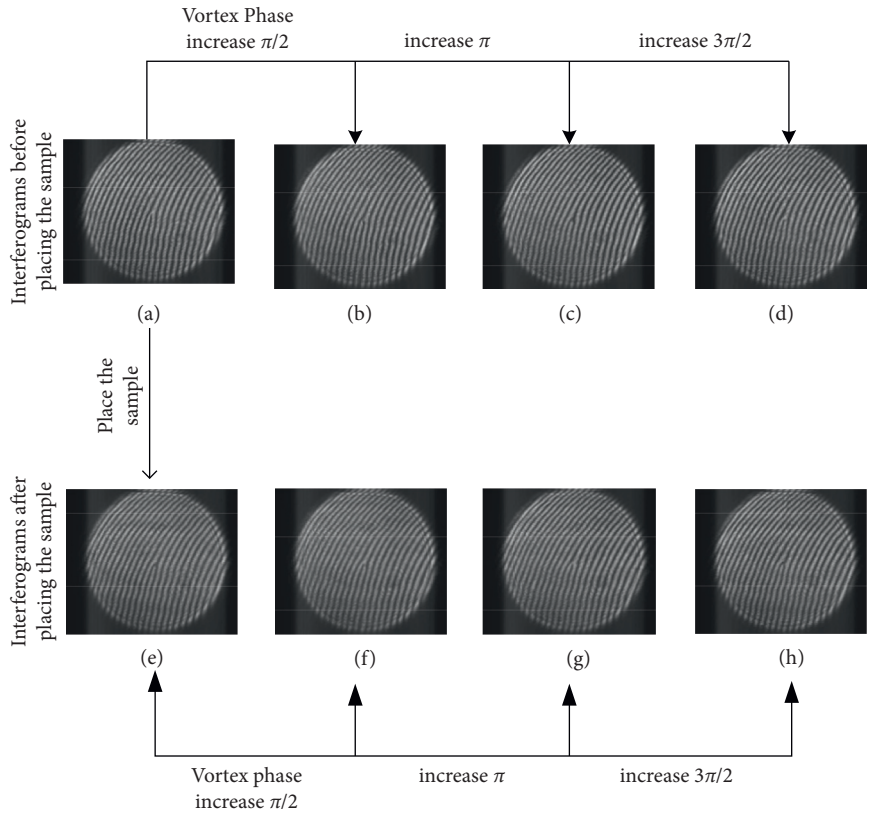

Figure 7: Interference patterns of +1 order vortex light and plane light. (a)–(d) Interferograms before placing the sample, and the phase of vortex light is (a) 0, (b) $\pi/2$, (c) π, and (d) $3\pi/2$. (e)–(h) Interferograms after placing the sample, and the phase of the vortex light is (e) 0, (f) $\pi/2$, (g) π, and (h) $3\pi/2$.

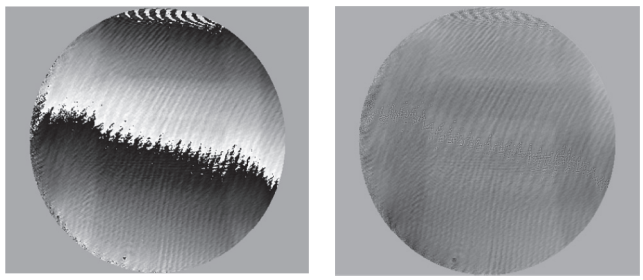

Figure 8: (a) Wrapped phase distribution. (b) Phase distribution after unwrapping.

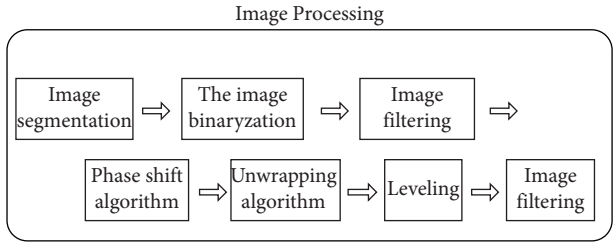

Figure 9: Flowchart of image processing in experiment.

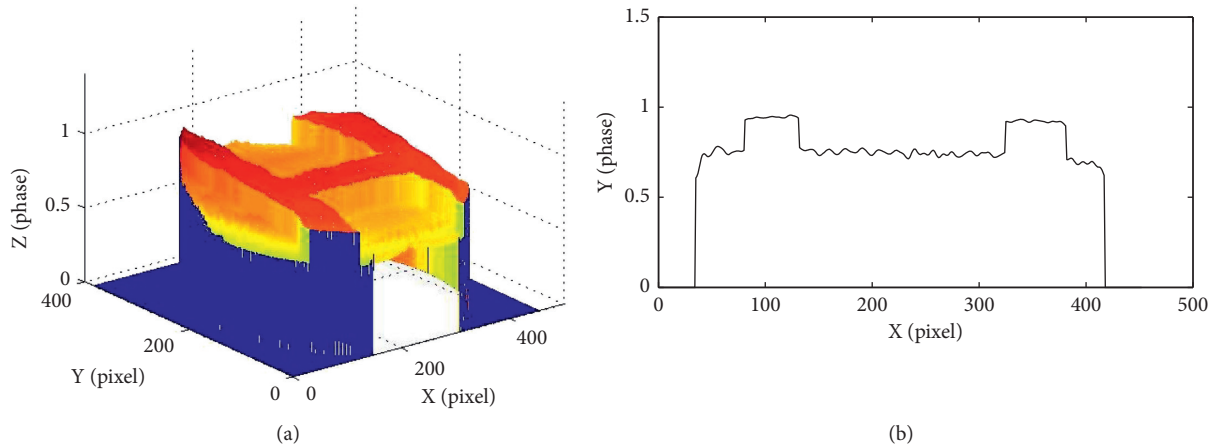

Figure 10: (a) Three-dimensional profile of the sample after unwrapping. (b) Phase value of the 170th line of the sample phase image.

that H-shape occupies in the picture and the pixel size of the CCD camera, the width of vertical stripes on the left and right sides of H-shape film is calculated to be 1.498 mm, and the length and width of the horizontal stripe in the middle are 4.729 mm and 1.498 mm, respectively. The calculated result is very close to the true value. The experimental and simulation results show that the optical vortex phase shift technique can be used to measure the surface profile of objects.

5. Conclusions

In conclusions, we have achieved a high-accuracy measurement of the transparent sample based on the vortex phase-shifting interferometry and analyzed the influence of the nonlinear phase modulation characteristics of the spatial light modulator on the measurement precision. The simulation of the nonlinear phase is operated by gamma transformation of vortex light phase diagram, and the results show that measurement error was positively correlated with the nonlinear phase. In the state of linear modulation of SLM, the profile of thin film was measured. The width of vertical stripes on the left and right sides of H-shape film is 1.498 mm, the length and width of the horizontal stripe in the middle are 4.729 mm and 1.498 mm, respectively, and the thickness of the sample is 18.854 nm, with an error of 1.146 nm compared with the theoretical value of 20 nm. Due to the limitations of the experimental environment (air vibration and equipment stability), as well as errors in the solution algorithm, there will be errors in the value of the solution phase. Because the thickness of the measured sample is a large value, the error of a certain partial thickness will not affect the estimation of the transverse dimensions, so the transverse dimensions can be accurately measured (error rate is 0.7%), and the measurement error in the vertical direction is larger (error rate is 5.7%).

Data Availability

The data used to support the findings of this study are included within the article.

Conflicts of Interest

The authors declare that there are no conflicts of interest.

Acknowledgments

The authors would like to express their sincere thanks to Mr. Shihong Jiang of the University of St. Andrews who provided valuable advice. This research was funded by the National Natural Science Foundation of China (62005254), Shanxi Province Science Foundation for Youths (201901D211280), and Scientific and Technological Innovation Programs of Higher Education Institutions in Shanxi (2019L0565).

References

[1] Y. Zhou, H. Gao, J. Teng, X. Luo, and M. Hong, "Orbital angular momentum generation via a spiral phase microsphere," *Optics Letters*, vol. 43, no. 1, pp. 34–37, 2018.

[2] P. S. Ruchi and S. K. Pal, "Phase singularities to polarization singularities," *International Journal of Optics*, vol. 2020, Article ID 2812803, 33 pages, 2020.

[3] Y. Shen, "Optical vortices 30 years on: OAM manipulation from topological charge to multiple singularities," *Light: Science & Applications*, vol. 8, no. 90, 2019.

[4] X. Hu, Q. Zhao, P. Yu et al., "Dynamic shaping of orbital-angular-momentum beams for information encoding," *Optics Express*, vol. 26, no. 2, pp. 1796–1808, 2018.

[5] J. Wang, "Advances in communications using optical vortices," *Photonics Research*, vol. 4, no. 5, pp. 14–28, 2016.

[6] W. Wei, K. Mahdjoubi, C. Brousseau, and O. Emile, "Generation of OAM waves with circular phase shifter and array of patch antennas," *Electronics Letters*, vol. 51, no. 6, pp. 442-443, 2015.

[7] X. Yan, L. Guo, M. Cheng, and J. Li, "Controlling abruptly autofocusing vortex beams to mitigate crosstalk and vortex splitting in free-space optical communication," *Optics Express*, vol. 26, no. 10, pp. 12605–12619, 2018.

[8] S. Fu, S. Zhang, T. Wang, and C. Gao, "Measurement of orbital angular momentum spectra of multiplexing optical vortices," *Optics Express*, vol. 24, no. 6, pp. 6240–6248, 2016.

[9] A. D'Errico, "Measuring the complex orbital angular momentum spectrum and spatial mode decomposition of

structured light beams," *Optica*, vol. 4, no. 11, pp. 1350–1357, 2017.

[10] S. N. Khonina, V. V. Podlipnov, S. V. Karpeev, A. V. Ustinov, S. G. Volotovsky, and S. V. Ganchevskaya, "Spectral control of the orbital angular momentum of a laser beam based on 3D properties of spiral phase plates fabricated for an infrared wavelength," *Optics Express*, vol. 28, no. 12, pp. 18407–18417, 2020.

[11] L. A. Shaw, C. M. Spadaccini, J. B. Hopkins, and J. B. Hopkins, "Scanning holographic optical tweezers," *Optics Letters*, vol. 42, no. 15, pp. 2862–2865, 2017.

[12] S. Bernet, A. Jesacher, S. Fürhapter, C. Maurer, and M. Ritsch-Marte, "Quantitative imaging of complex samples by spiral phase contrast microscopy," *Optics Express*, vol. 14, no. 9, pp. 3792–3805, 2006.

[13] M. P. J. Lavery, F. C. Speirits, S. M. Barnett, and M. J. Padgett, "Detection of a spinning object using light's orbital angular momentum," *Science*, vol. 341, no. 6145, pp. 537–540, 2013.

[14] I. Fujimoto, M. Y. Sato, S. Sato, M. Y. Kim, and S. Ando, "Optical vortex beams for optical displacement measurements in a surveying field," *Measurement Science and Technology*, vol. 22, no. 10, pp. 105301–105311, 2011.

[15] M. V. Berry, "Optical vortices evolving from helicoidal integer and fractional phase steps," *Journal of Optics A: Pure and Applied Optics*, vol. 6, no. 2, pp. 259–268, 2004.

[16] S. N. Khonina, "Properties of vortex light fields generated by generalized spiral phase plates," *Physical Review A*, vol. 101, no. 4, Article ID 043829, 2020.

[17] N. L. Kazanskiy, S. N. Khonina, S. V. Karpeev, and A. P. Porfirev, "Diffractive optical elements for multiplexing structured laser beams," *Quantum Electronics*, vol. 50, no. 7, pp. 629–635, 2020.

[18] S. S. R. Oemrawsingh, E. R. Eliel, J. P. Woerdman, E. J. K. Verstegen, J. G. Kloosterboer, and G. W. 't Hooft, "Production and characterization of spiral phase plates for optical wavelengths," *Applied Optics*, vol. 43, no. 3, pp. 688–694, 2004.

[19] S. N. van Houwelingen, A. P. Porfirev, and A. V. Ustinov, "Diffraction patterns with mth order symmetry generated by sectional spiral phase plates," *Journal of Optics*, vol. 17, no. 12, 2015.

[20] V. V. Kotlyar, A. A. Kovalev, R. V. Skidanov, S. N. Khonina, O. Y. Moiseev, and V. A. Soĭfer, "Simple optical vortices formed by a spiral phase plate," *Journal of Optical Technology*, vol. 74, no. 10, pp. 686–693, 2007.

[21] Z. Zhang, F. Dong, K. Qian et al., "Real-time phase measurement of optical vortices based on pixelated micropolarizer array," *Optics Express*, vol. 23, no. 16, pp. 20521–20528, 2015.

[22] C.-S. Guo, X. Cheng, X.-Y. Ren, J.-P. Ding, and H.-T. Wang, "Optical vortex phase-shifting digital holography," *Optics Express*, vol. 12, no. 21, pp. 5166–5171, 2004.

[23] B. Sokolenko, D. Poletaev, and S. Halilov, "Phase shifting profilometry with optical vortices," *Journal of Physics: Conference Series*, vol. 917, no. 6, 2017.

[24] H. Sun, X. Wang, and P. Sun, "In-plane displacement measurement using optical vortex phase shifting," *Applied Optics*, vol. 55, no. 21, pp. 5610–5613, 2016.

[25] X. Zhang, J. Zhang, Y. Zhang, D. Liu, and J. Zhu, "Phase-shifting image-plane digital holography with elliptical vortex sieve," *Optics & Laser Technology*, vol. 115, pp. 359–363, 2019.

[26] W.-P. Wang, S.-J. Huang, Y. Chen, J.-W. Wang, and C. Yan, "Three-dimensional refractive index measurement of special optical fiber based on optical vortex phase-shifting digital holographic microscopy," *Optical Engineering*, vol. 58, no. 3, Article ID 034108, 2019.

[27] J. Masajada, M. Leniec, E. Jankowska, H. Thienpont, H. Ottevaere, and V. Gomez, "Deep microstructure topography characterization with optical vortex interferometer," *Optics Express*, vol. 16, no. 23, pp. 19179–19191, 2008.

[28] A. Serrano-Trujillo, M. E. Anderson, and M. E. Anderson, "Surface profilometry using vortex beams generated with a spatial light modulator," *Optics Communications*, vol. 427, pp. 557–562, 2018.

[29] I. D. Maleev and G. A. Swartzlander Jr., "Composite optical vortices," *Journal of the Optical Society of America B*, vol. 20, no. 6, pp. 1169–1176, 2003.

[30] X. Hu, Z. Gezhi, O. Sasaki, Z. Chen, and J. Pu, "Topological charge measurement of vortex beams by phase-shifting digital hologram technology," *Applied Optics*, vol. 57, no. 35, pp. 10300–10304, 2018.

[31] K. I. T. Remulla and N. Hermosa, "Spatial light modulator phase calibration based on spatial mode projection," *Applied Optics*, vol. 58, no. 21, pp. 5624–5630, 2019.

[32] Y. Li and J. Zhang, "Radial-shearing interferometry for phase LC-SLM calibration with a pair of conjugated vortex beams," *Journal of Optics*, vol. 22, no. 2, 2020.

[33] R. Stephan, "Spatially resolved phase-response calibration of liquid-crystal-based spatial light modulators," *Applied Optics*, vol. 52, no. 12, pp. 2610–2618, 2013.

[34] H. van Brug, "Phase-step calibration for phase-stepped interferometry," *Applied Optics*, vol. 38, no. 16, pp. 3549–3555, 1999.

[35] Y. Jiang, H. Liu, L. Wang et al., "Optical and interfacial layer properties of SiO2 films deposited on different substrates," *Applied Optics*, vol. 53, no. 4, pp. A83–A87, 2014.

[36] M. A. Navarro, J. C. Estrada, M. Servin, J. A. Quiroga, and J. Vargas, "Fast two-dimensional simultaneous phase unwrapping and low-pass filtering," *Optics Express*, vol. 20, no. 3, pp. 2556–2561, 2012.